Merging of spin-wave modes in obliquely magnetized circular nanodots

Julia Kharlan,[1,*] Vladyslav Borynskyi,[1,*] Sergey A. Bunyaev,[2] Pavlo Bondarenko,[1] Olga Salyuk,[1] Vladimir Golub,[1] Alexander A. Serga,[3] Oleksandr V. Dobrovolskiy,[4] Andrii Chumak,[4] Roman Verba,[1,†] and Gleb N. Kakazei[2]

[1]*Institute of Magnetism, Kyiv 03142, Ukraine*

[2]*Institute of Physics for Advanced Materials, Nanotechnology and Photonics (IFIMUP), Departamento de Fisica e Astronomia, Universidade do Porto, 4169-007 Porto, Portugal*

[3]*Fachbereich Physik and Landesforschungszentrum OPTIMAS, Technische Universität Kaiserslautern, Kaiserslautern 67663, Germany*

[4]*Faculty of Physics, University of Vienna, 1090 Vienna, Austria*

(Received 9 November 2021; revised 18 December 2021; accepted 23 December 2021; published 5 January 2022)

Magnetic nanoelements attract great interest due to their prospects for data storage and signal processing. Spin-wave confinement in these elements implies wave-number quantization, discrete frequency spectra and thus complex resonance patterns, strongly dependent on the elements' geometry and static magnetic configuration. Here we report experimental observation of unconventional single-frequency resonance response of flat circular Permalloy nanodots, which is achieved via the application of a magnetic field at a certain critical angle $\tilde{\theta}_B$ with respect to the dot normal. This observation is explained as the merging of spin-wave eigenmodes under the transition of the spin-wave dispersion from the forward-volume to the backward-volume type, as elucidated by micromagnetic simulations in conjunction with an analytical theory. Our results offer a way for the creation of spin-wave systems with spectrally narrow magnetic noise.

DOI: 10.1103/PhysRevB.105.014407

I. INTRODUCTION

The spectrum and structure of linear spin-wave (SW) eigenmodes are among the most important dynamic characteristics of magnetic micro- and nanoelements (e.g., nanodots, stripes, nanowires, etc.). Indeed, SW modes define the response of an element to a microwave magnetic field or spin current [1,2], stability of a static magnetization configuration and, in the case of instability, the type of this instability [3]. Nonlinear and parametric processes are also sensitive to the structure and symmetry of SW modes [4–6]. The interplay of magnetic interactions (exchange, dipolar, Zeeman, and anisotropy) results in a great variety of ground states and metastable magnetic configurations in patterned magnetic structures, which are strongly dependent on their shape and applied magnetic field. Herewith the static magnetic state together with quantization conditions, defined by dot geometry, crucially affect the SW mode structure and spectrum. This strong effect allows for the engineering of magnetic nanoelements with specific features of SW spectrum, required for applications.

Almost two decades of intensive investigation of SW modes in patterned magnetic structures have provided a deep understanding of SW mode features in many important cases. Simultaneously, it should be noted that the majority of works was focused on highly symmetric structures, e.g., circular [7–13], rectangular [14–16], elliptic [17,18] flat magnetic dots, regular triangular prisms and pyramids [19], spheres [20], rings [21–24], emerging 3D structures like nanovolcanoes [25], etc. Considered magnetization configurations were also symmetric: the quasiuniform state [7,10,14–18], the vortex state [8,9,11], skyrmions [26,27], etc. Deviations from a symmetric case, both in geometry and magnetization configuration, were often considered as undesirable. Such deviations typically complicate the identification and classification of SW modes, lead to mode splitting, and sophisticate the overall SW spectrum [28,29].

Recent works [5,30,31], however, have demonstrated, that breaking of geometric and/or magnetic state symmetry can result in the appearance of new qualitative features, which cannot be observed in a symmetric case. For instance, in one of the simplest structure—micron-thick magnetic film—a tilt of the bias magnetic field from the film plane results in the appearance of quasitraveling SW modes (instead of standard perpendicular standing SW modes, PSSWs), which, in particular, could transfer spin current across the film thickness [30]. Similar in nature modes were observed in relatively thick magnetic nanodisks in vortex state, where the symmetry becomes broken due to large demagnetization fields of the vortex core [31]. Also, it has been revealed that a violation of magnetic symmetry is a crucial point to remove a restriction on degenerate three-magnon splitting and confluence processes thus allowing control of nonlinear magnetic damping [5].

Here we introduce another interesting phenomenon arising under the violation of magnetic state symmetry. We study the evolution of spin-wave resonance (SWR) spectra of flat (height-to-diameter aspect ratio $h/D \ll 1$) circular magnetic dots in a saturated state when the external magnetic field is tilted with respect to the dot plane normal. Although at small deviation angles SW modes split, like it was shown previously

*These authors contributed equally to the work.
†verrv@ukr.net

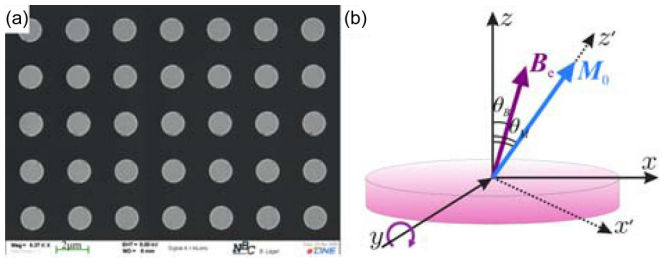

FIG. 1. (a) Scanning electron microscopy image of the array of Permalloy cylindrical dots with dot diameter $D = 1500$ nm, thickness $h = 40$ nm, and center-to-center interdot distance of 3000 nm. (b) Sketch of a circular magnetic dot with the indicated directions of bias magnetic field $\boldsymbol{B}_e$ and static magnetization $\boldsymbol{M}_0$, and coordinate systems used in the text.

[28], we demonstrate that there exists a critical angle at which an unexpected regularization of the resonance spectra occurs and the spectra become effectively single frequency. Such spectral features could be useful, for example, for the creation of SW systems with spectrally narrow magnetic noise.

The paper is organized as follows. Experimental details and results are discussed in Sec. II. Section III presents micromagnetic simulations of the resonance spectra and SW mode structures. A theoretical model explaining the main experimental findings is introduced in Sec. IV. Finally, the obtained results are summarized in Sec. V.

II. EXPERIMENTAL RESULTS

The set of square arrays of circular Permalloy ($Ni_{80}Fe_{20}$) dots was fabricated on a Si wafer with an oxidized surface; the details of sample preparation are presented elsewhere [28]. The magnetic nanoelements have the following dimensions: The dot thickness $h = 40$ nm for all the arrays and the dot diameters D are 500, 750, 1500, 2000, and 4000 nm. The center-to-center distance for all the arrays is equal to $2D$, which is large enough to neglect the influence of interdot dipolar interactions on the magnetization dynamics. Each sample contains a small unpatterned area with continuous film used for the determination of the film magnetic parameters: Saturation magnetization M_s and gyromagnetic ratio γ. A scanning electron microscopy image of the array of dots with $D = 1500$ nm is shown in Fig. 1(a).

SWR measurements were carried out at room temperature at the frequency 9.85 GHz using a standard electron-spin-resonance spectrometer Bruker ELEXYS E500. The SWR spectra were measured for different angles θ_B between the external magnetic field $\boldsymbol{B}_e$ and the dot normal. The angle θ_B was varied in the range $0 - 14^\circ$ with a step of 0.25° using an automatic goniometer. The experimental geometry is shown in the Fig. 1(b) and the SWR spectra for dot arrays with $D = 500$, 1500, and 4000 nm are shown in Fig. 2 for the series of θ_B. In the case of external field applied along the dot normal ($\theta_B = 0^\circ$), well-known SW spectra for perpendicularly magnetized cylindrical dots were observed [7]. These spectra were perfectly fitted using an analytical theory that suggests Bessel functions of first kind as spin-wave mode profiles [7]. The small peak at a higher field B_e of 1.32 T for all the samples corresponds to the reference continuous film area.

At small deviations of magnetic field from the dot normal ($\theta_B \sim 1^\circ - 4^\circ$) a splitting of the SW modes is observed, which is in line with previous studies [28]. Please note that it is difficult to distinguish the splitting in Fig. 2 due to the scale used. However, at larger angles the spectra change in a qualitatively different way. At small θ_B the mode splitting makes the SWR spectra even more complex, but near a certain angle $\tilde{\theta}_B$ (which is called the "critical angle" below) the spectra become much more regular and contain only one intensive resonance peak [see the resonance spectra for $\theta_B = 6.5^\circ$ and $\theta_B = 6^\circ$ in Figs. 2(b) and 2(c), respectively]. In other words, a microwave response of the dots becomes effectively single mode. Such a regularization and simplification of the SWR spectra is quite unexpected for this geometry with definitely broken symmetry. Obviously, this phenomenon cannot be explained within the perturbation framework used in Ref. [23] since it is valid for very small angles only. Apart from fundamental interest, this intriguing phenomenon could be useful for practical applications of patterned magnetic elements, i.e., in read-write magnetic heads, magnetic random access memory cells, microwave detectors, etc. In such devices, additional SW modes can be considered as magnetic noise [32] and the proper selection of external magnetic field direction may lead to the minimization of such a noise contribution.

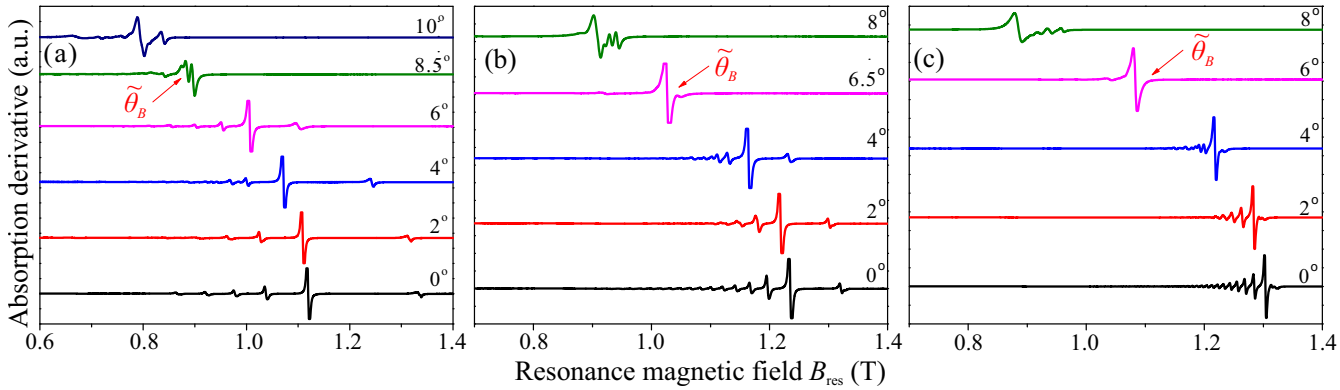

FIG. 2. Experimental SWR spectra of the dot arrays for different angles of the applied static magnetic field; $\tilde{\theta}_B$ is the critical angle at which the system behaves as almost that of a single mode. Dot diameters are $D = 500$ nm (a), $D = 1500$ nm (b), and $D = 4000$ nm (c).

At even larger bias field angles $\theta_B > \tilde{\theta}_B$, the SWR spectra also contain several resonance peaks. However, the position of higher-order modes with respect to the main one (the most intensive) changes; while below the critical angle ($\theta_B < \tilde{\theta}_B$) the resonance fields of higher-order modes are lower than that of the main mode (i.e., higher-order modes have larger frequencies at a constant field), above the critical angle ($\theta_B > \tilde{\theta}_B$) higher-order peaks are located at larger fields respective to the main one. Also, it is revealed that the critical angle $\tilde{\theta}_B$ slightly decreases with an increase of the dot diameter. It should also be mentioned that this effect is much more pronounced for larger dots. Particularly, a nearly perfect single-peak SWR spectrum is observed for the dots with $D = 1500$ nm and $D = 4000$ nm, while in the case of smallest dot diameter $D = 500$ nm, in the best case the spectrum contains two closely located resonance peaks [see the spectrum for $\theta_B = 8.5^\circ$ in Fig. 2(a)].

It should be pointed out that a similar investigation (SWR of obliquely magnetized circular dots) was carried out in Ref. [33]; however, the lack of systematic measurements of the angular dependences did not allow for observations of the phenomenon of mode merging.

III. MICROMAGNETIC SIMULATIONS

In general, a tilt of magnetic field from the perpendicular to the dots plane direction leads to several qualitative changes, which may be responsible for the observed phenomenon of the disappearance of higher-order resonance peaks in the SWR spectra. First (i) the profile of the static internal magnetic field inside a dot changes. Indeed, in the case of a perpendicular magnetic field ($\theta_B = 0$), the demagnetization field forms a potential hill near the dot edges and, as a result, the SW mode amplitude at the dot edge is close to zero (i.e., SW modes are almost fully pinned) [7]. In contrast, when the field is in the dot plane, two potential wells are formed near the dot edges, and the so-called edge modes, localized in these wells, appear, while the other modes ("volume modes") are formed outside these wells [8–10]. Another mechanism, which also strongly affects the mode profiles, is (ii) the effective dipolar pinning. This mechanism is a consequence of the dynamic demagnetization field effect in flat patterned magnetic structures [34,35]. As only one dynamic magnetization component—in-plane perpendicular to an edge—is responsible for this pinning mechanism [36], it is clear that the effect of dipolar pinning is also sensitive to the direction of static magnetization. Both mechanisms affect the mode profiles and one may expect the transformation of higher-order SW mode profiles into those with a vanishing net magnetic moment, which, obviously, makes such modes invisible in SWR spectra. Such a situation can take place, for instance, in the case of rectangular magnetic dots with an almost uniform internal magnetic field without a pinning at the edges (free boundary condition) [37]. The last evident mechanism is (iii) a transformation of the SW spectrum under the field tilt, which, possibly, could result in a degeneracy of the most intensive SW modes.

To obtain a first insight into the nature of the observed phenomenon, a series of micromagnetic simulations using MuMax3 software [38] has been performed. The results for the dots with diameter $D = 1500$ nm are presented here.

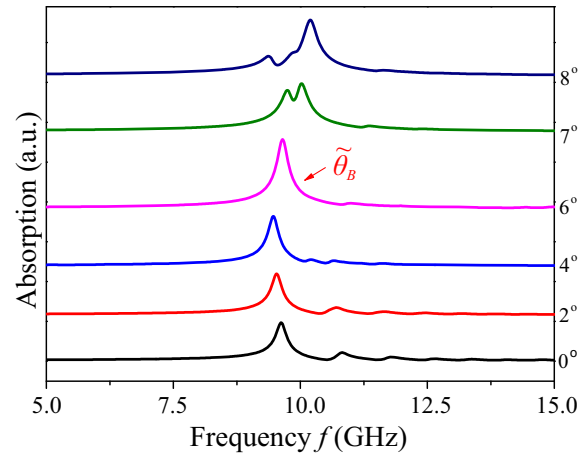

FIG. 3. Simulated resonance spectra for a dot with $D = 1500$ nm for a series of tilt angles of the bias field, including the critical angle $\tilde{\theta}_B$.

The simulations for $D = 2000$ nm and $D = 500$ nm reveal the same qualitative features. The cell size in the simulations was set to $5.86 \times 5.86 \times 40\,\text{nm}^3$, and the standard Permalloy parameters were used in the simulations, namely, the saturation magnetization $M_s = 810 \times 10^3$ A/m, the exchange stiffness $A = 10.5 \times 10^{-12}$ J/m, and the gyromagnetic ratio $\gamma = 2\pi \times 29.6$ GHz/T. Since the simulations of SWR spectra with a field sweep (as in the experiment) are excessively time consuming, we instead simulate the frequency spectra under a constant bias field using the standard technique of pulse excitation followed by the Fourier transformation of the magnetization dynamic time evolution. The excitation field pulse is, obviously, spatially homogeneous. The magnitude of the bias field was set to the experimentally measured resonance field of the most intensive mode at a given field angle.

The simulated spectra are presented in Fig. 3. Because of the finite accuracy of the simulation data it is difficult to obtain the derivative of the spectra (like in Fig. 2) without undesirable smoothing; therefore the spectra rather than their derivatives are shown in Fig. 3. There is a quite good correlation between the experimental and the simulated positions of the main mode. Some small deviations from the experimental value of 9.85 GHz are due to some difference of the magnetic parameters for real samples from those used in the simulations. Yet the results of micromagnetic simulations qualitatively reproduce the main peculiarities observed in the experiment. Indeed, at the critical angle $\tilde{\theta}_B = 6^\circ$ only one peak is present in the SWR spectrum and there are no higher-order modes. It is worth noting that the experimental value of the critical angle $\tilde{\theta}_B$ for $D = 1500$ nm [Fig. 2(b)] is quite close to $\tilde{\theta}_B = 6^\circ$ obtained in the simulations. Another important observation is the significant decrease in the distances between the most intensive and higher-order peaks when the bias field angle is approaching $\tilde{\theta}_B$ (at least for the 2nd, 3rd, and 4th peaks). This observation is the key feature to explain the observed phenomenon of resonance spectra simplification, as will be discussed below.

Using the single-frequency excitation technique (see, e.g., Ref. [31]), profiles of SW modes were obtained. The profiles

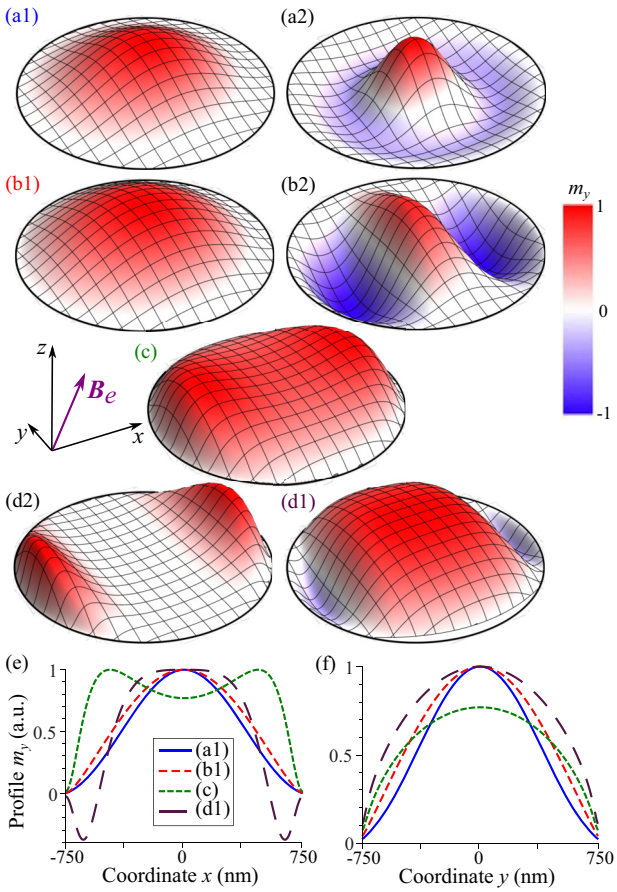

FIG. 4. Simulated profiles (normalized dynamic component m_y) of the two most intensive modes in the SWR spectra for a series of field tilt angles: (a) $\theta_B = 0$, (b) $\theta_B = 4^\circ$, (c) $\theta_B = 6^\circ$, and (d) $\theta_B = 7^\circ$; the left column depicts the lower frequency mode; the right column corresponds to the higher frequency mode; indices 1 and 2 correspond to the first and second in intensity modes, respectively. At $\theta_B = \tilde{\theta}_B = 6^\circ$ only one mode (c) is visible in the SWR spectrum. Panels (e) and (f) show central cross-sections of the mode profiles along the x and y directions, respectively, for the most intensive mode (mode 1).

are shown in Fig. 4 for the two most intensive modes. At $\theta_B = 0$ these are the well-known cylindrical modes whose profiles are described by Bessel's functions $J_0(k_n r)$. At a small tilt of the field direction with respect to the dot normal, the cylindrical symmetry for the most intensive mode is almost preserved [Fig. 4(b1)]. Another situation is for higher-order modes, which acquire Cartesian symmetry and become backward volume magnetostatic wave (BVMSW)-like standing modes. Figure 4(b2) shows the 3rd BVMSW-like mode; the other distinguishable peaks in the SWR spectrum at $\theta_B = 4^\circ$ correspond to the 5th and 7th modes, respectively. The modes with odd profiles (the 2nd, 4th, 6th, etc. modes) are not visible in the SWR spectrum because they are fully antisymmetric. The excitation profile at the critical angle $\tilde{\theta}_B = 6^\circ$ is rather uncommon and resembles a superposition of several modes [Fig. 4(c)], namely, a superposition of the modes shown in the panels (b1) and (b2) or (d1) and (d2) with certain weights. A detailed explanation of this will be presented in Sec. IV. Finally, at angles exceeding the critical one $\tilde{\theta}_B$ the observed peaks correspond to quasiuniform and symmetric edge modes [Figs. 4(d1) and 4(d2), respectively].

It is important to mention, that, according to the simulations, at all bias field angles the SW modes remain rather strongly pinned at the dot edges. Even the edge mode is pinned. Some weak unpinning takes place only at the dot edges, parallel to the in-plane field projection [see mode profiles cross-sections in Fig. 4(f)]. This means that the potential scenario of the mode unpinning, mentioned at the beginning of this section, is not realized and cannot be responsible for the disappearance of resonance peaks in the SWR spectra.

IV. THEORETICAL MODEL

To proceed further with the understanding of the experimentally observed phenomena, we build a simple analytical model for the description of the SW spectrum in an obliquely magnetized circular nanodot. A theory of the SW mode spectrum and structure is well developed for the case of perpendicular static magnetization [7]. In the case of an oblique magnetization the problem of SW eigenmodes becomes too complex, and to date only a perturbation theory exists, which is valid for small deviations of the magnetization angle from the dot normal [28].

In our case, in the range of interest, i.e., in the vicinity of the critical-field angle $\tilde{\theta}_B$, the deviation of the static magnetization direction from the dot normal direction is large enough [$\theta_M \sim 30^\circ$, see Fig. 6(c)], and perturbation approaches are not applicable. The SW modes completely lose cylindrical symmetry and acquire approximately Cartesian symmetry with the axes defined by the in-plane projection of the static magnetization (and the bias field). This feature is known for in-plane magnetized circular dots [8,9]. Indeed, in this case an attempt to describe the SW modes based on cylindrical Bessel's functions fails [39]. A complex but sufficiently accurate semianalytical theory of the SW modes can be built [40] only taking into account Cartesian symmetry, determined by the static magnetization direction and applying approximate boundary conditions (which, naturally, possess cylindrical symmetry).

Instead of building a cumbersome rigorous semianalytical theory like in Ref. [40], here we provide a simple estimation of the SW mode positions based on the lateral quantization of propagating SWs in a thin film (here and below "thin" refers to film thickness of several exchange lengths and below, in which dynamic magnetization is almost uniform across the film thickness). The SW dispersion law in a thin film is well known [41,42]:

$$\omega_{\boldsymbol{k}}^2 = \left(\omega_H + \omega_M \lambda_{\text{ex}}^2 k^2 + \omega_M F_{\boldsymbol{k}}^{(x'x')}\right) \times \left(\omega_H + \omega_M \lambda_{\text{ex}}^2 k^2 + \omega_M F_{\boldsymbol{k}}^{(yy)}\right). \quad (1)$$

Here we omit the off-diagonal term as such an off-diagonal term always vanishes in a finite magnetic system, e.g., magnetic stripes, rectangular nanodos, etc. [42]. In Eq. (1) $\omega_H = \gamma B$, B is the modulus of the static internal magnetic field in the dot, $\omega_M = \gamma \mu_0 M_s$, $\lambda_{\text{ex}} = \sqrt{2A/\mu_0 M_s^2}$ is the exchange length; $k^2 = k_x^2 + k_y^2$, $F_{\boldsymbol{k}}^{(x'x')} = F_{\boldsymbol{k}}^{(xx)} \cos^2\theta_M + F_{\boldsymbol{k}}^{(zz)} \sin^2\theta_M$ is the component of the dynamic demagnetization tensor in the rotated coordinate system $(x'yz')$ with z' axis along the static

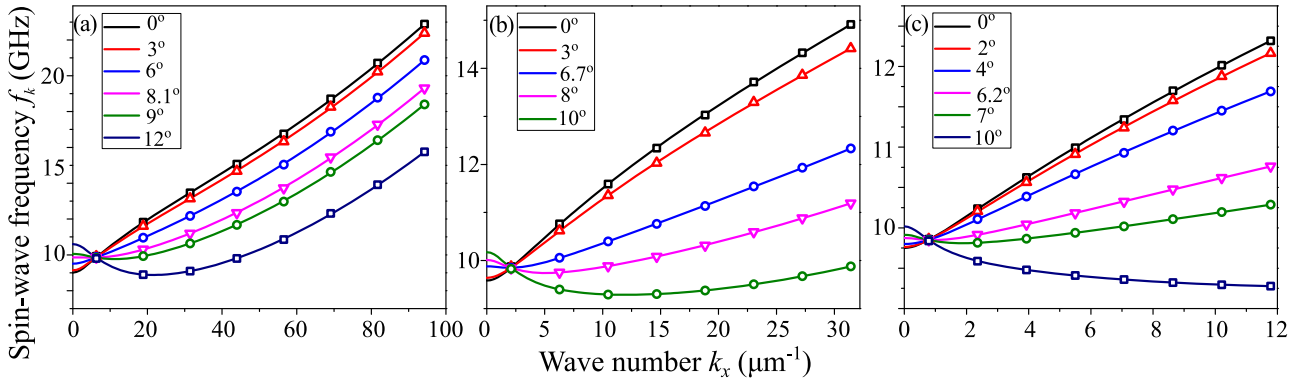

FIG. 5. Theoretically calculated SW dispersion $f_{k_x} = (1/2\pi)\omega(k_x)|_{k_y=\pi/D}$ for a series of tilt angles of the applied field and different dot diameters: (a) $D = 500$ nm, (b) $D = 1500$ nm, and (c) $D = 4000$ nm. Symbols denote the position of odd standing SW modes $(n, 1)$ which should be visible in the SWR spectra. The value of the external magnetic field for each angle was chosen to preserve constant frequency of the fundamental mode $f_{\pi/D}$.

magnetization direction [see Fig. 1(b)]. In the "natural" coordinate system (xyz) tensor $\hat{\boldsymbol{F}}_{\boldsymbol{k}}$ is equal to

$$\hat{\boldsymbol{F}}_{\boldsymbol{k}} = \begin{pmatrix} k_x^2 f/k^2 & k_x k_y f/k^2 & 0 \\ k_x k_y f/k^2 & k_y^2 f/k^2 & 0 \\ 0 & 0 & 1-f \end{pmatrix}, \tag{2}$$

where $f = 1 - (1 - e^{-|kh|})/|kh|$. The value of both the static internal magnetic field B and the magnetization angle θ_M is found in the approximation of uniform static magnetization distribution from the system of equations

$$\begin{cases} B\cos\theta_M = B_e\cos\theta_B - \mu_0 M_s N_{zz}\cos\theta_M \\ B\sin\theta_M = B_e\sin\theta_B - \mu_0 M_s N_{xx}\sin\theta_M, \end{cases} \tag{3}$$

with $N_{xx} = N_{yy} = (1 - N_{zz})/2$ and

$$N_{zz} = \frac{2}{h}\int_0^\infty \frac{(1-e^{-qh})J_1^2(qR)}{q^2}dq \approx 1 - \frac{h}{\pi R}\left(\log\frac{8R}{h} - \frac{1}{2}\right) \tag{4}$$

being the components of the static demagnetization tensor of a circular nanodot [43]. Here the approximation in the right-hand side is valid for $h \ll R = D/2$ [44].

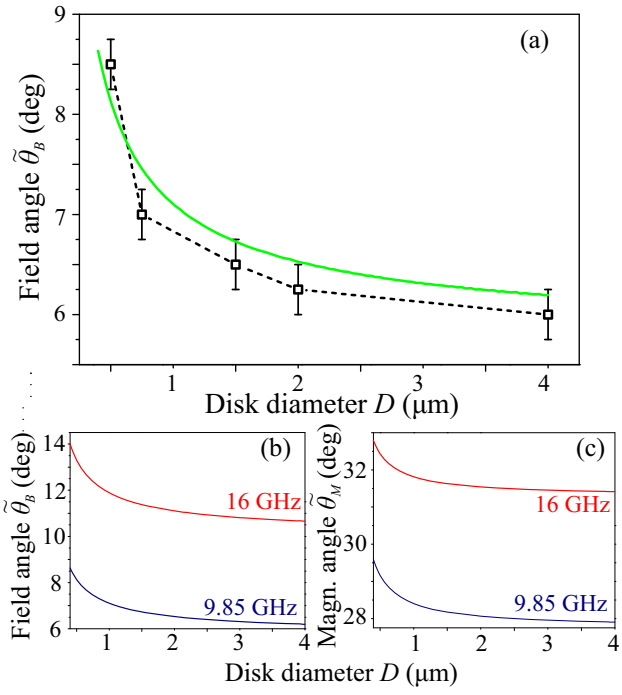

FIG. 6. (a) Experimental (dots) and theoretical (solid line) dependence of the critical angle $\tilde{\theta}_B$ on the dot diameter. Panels (b) and (c) show the theoretical dependencies of the critical field angle $\tilde{\theta}_B$ and the corresponding critical magnetization angle $\tilde{\theta}_M$ for different frequencies of the main (1,1) mode (i.e., different frequencies of the SWR measurements setup).

According to the micromagnetic simulations revealing strong pinning of the dynamic magnetization at the lateral edges, quantized wave numbers of the SW modes can be estimated as $k_x^{(n)} = \pi n/D$ and $k_y^{(m)} = \pi m/D$, where n, $m = 1, 2, 3, \ldots$ are the mode numbers. The modes with odd profiles (even mode numbers n or/and m) cannot be observed in the SWR spectra. Also, only modes with no nodes in the y direction are observed in the micromagnetic simulations since all other modes should have a small peak intensity and they are located at significantly higher frequencies (lower resonance fields) than the fundamental mode. Therefore attention below will only be paid to $(n, 1)$ modes with $n = 1, 3, 5, \ldots$.

The dispersion relations $\omega = \omega(k_x)|_{k_y=\pi/D}$, calculated within the described approach are shown in Fig. 5 for nanodots with different diameters D and for different angles θ_B (material parameters are the same as in the simulations). Herewith the diameter affects the fixed value of wave-number $k_y = \pi/D$. The positions of the quantized SW modes $(n, 1)$, which should be visible in the SWR spectra are marked on the dispersion plots. The value of the external magnetic field was chosen in such a way that the frequency of (1,1) mode remains the same, $\omega_{(1,1)}/2\pi = 9.85$ GHz. Theoretical resonance fields of the main mode calculated within this approach appear to be quite close to the experimental values, the discrepancy is within 5%, which additionally underlines reasonable accuracy of the theoretical model used.

For the magnetic field applied perpendicularly to the dots plane ($\theta_B = 0$) the dispersions are, naturally, forwardlike (SW frequency increases with k_x). When the field starts to deviate

from the normal, the dispersions transform to the backward-like type (SW frequency decreases with k_x). At a certain angle in between a part of the dispersion becomes almost flat, see, e.g., the curves for $\theta_B = 6.2^\circ$ and $\theta_B = 7^\circ$ in Fig. 5(c), which are almost flat in the range of $k_x \sim 0 - 2\,\mu\text{m}^{-1}$ and $k_x \sim 1 - 5\,\mu\text{m}^{-1}$, respectively. If several SW modes with quantized wave-numbers $k_x^{(n)}$ are within such flat range, their frequencies become very close to each other. Of course, mode hybridization (mode repulsion) does not allow several modes to have exactly the same frequencies, but the difference could become small in comparison with the resonance linewidth, and the corresponding modes cannot be distinguished from SWR measurements.

The mode merging is more pronounced for dots with larger diameters (see Fig. 5). Indeed, the quantized SW modes of the largest dot are most closely located in the k space. The distance between the neighboring odd $(n, 1)$ modes is $\Delta k_x = 2\pi/D$. The curvature of the dispersion and consequently the size of the flat range is determined mainly by the dot thickness and the exchange length and is weakly dependent on the diameter (see note on the influence of the diameter below). Thus the larger the dot diameter the more modes fall into the flat region and have indistinguishable frequencies. For instance, the resonance linewidth for Permalloy at the investigated frequencies is about 200–300 MHz and, as it follows from Fig. 5, for $D = 4000$ nm up to 6 modes can be situated within the linewidth-determined frequency range at the optimal angle, while for $D = 500$ nm only two modes fall into this frequency interval.

This picture is in full agreement with our experimental observation and micromagnetic simulations. Indeed a decrease of the intermode distance is observed when the angle is approaching the critical value $\tilde{\theta}_B$. At the angles larger then $\tilde{\theta}_B$, higher-order resonance peaks change their position respective to the most intensive one (lower frequency or higher resonance fields, respectively, see Figs. 2 and 3). Finally, at $\tilde{\theta}_B$ the mode profile exhibits clearly a mixed or hybridized structure (Fig. 4). All these characteristic features follow from the theoretical model taking into account that in a real experiment it is possible to observe only a few first SW modes (with the lowest mode indices n). Higher-order modes have a too small overlap with a uniform excitation field, i.e., the excitation efficiency of these modes decreases sharply with increasing mode number, as can be seen in Fig. 2. Thus we conclude that the underlying nature of the observed phenomenon of resonance spectra transition from multimode to effectively single mode is the approximate degeneracy of the most intensive modes during the transition from forwardlike to a backwardlike SW dispersion.

In principle, one could imagine several different criteria for the calculation of the critical angle $\tilde{\theta}_B$ from the theoretical dispersion relations. Here we use the following: Flatness (i.e., zero first derivative) of the dispersion at the position of the fundamental mode (1,1),

$$\left.\frac{\partial \omega_{\boldsymbol{k}}}{\partial k_x}\right|_{k_x = k_y = \pi/D} = 0. \tag{5}$$

Using this criterion, we calculate the dependence of the critical angle $\tilde{\theta}_B$ on the dot diameter, which is in quite good agreement with the experimental data [Fig. 6(a)], especially as for such an approximate theory.

Here two important points should be addressed. First, the transition of the SW dispersion in magnetic films from forward to backward is, of course, well known. However, in a thin film it takes place at a different angle than the one observed here for nanodots. One can easily find setting $k_y = 0$ in Eq. (1) that the SW group velocity in the x direction at small k, $v_{gr} = \partial\omega_k/\partial k_x|_{k_x \to 0}$, turns to zero at the magnetization angle $\theta_M = 45^\circ$. The magnetization angle, corresponding to the SW mode merging [see Fig. 6(c)], is evidently smaller. This is a consequence of a nonzero transversal wave number of the quantized SW modes $k_y = \pi/D$, which is also responsible for the dependence of the critical angle $\tilde{\theta}_M$ on the dot size [Fig. 6(c)]. The size dependence of the corresponding field angle $\tilde{\theta}_B$ is somewhat strengthened by the additional size dependence of the static demagnetization factors of a dot.

The second point is that we use formalism for volume modes and completely disregard edge modes. Therefore such a consideration is valid only if the mode merging takes place at smaller field (and magnetization) tilts comparing to one at which static demagnetization leads to the formation of field wells at the dot edges with a subsequent appearance of edge modes. In our case, these phenomena take place at quite close angles, but the angle of formation of well-defined edge modes is larger than the angle of the mode merging (see Fig. 4). In the general case, the formation of field wells at the dot edges takes place close to the $\theta_M = 45^\circ$ magnetization angle. Indeed, near the edges, which are perpendicular to the x direction, the yy component of the spatially dependent demagnetization tensor is weak and other components $N_{xx}(x) \approx 1 - N_{zz}(x)$. The N_{zz} component favors the formation of a field hill at the edge, while the xx component is responsible for the formation of a field well. At $\theta_M = 45^\circ$ they compensate each other and a uniform internal field profile is expected. In a real circular dot, the picture is somewhat more complicated due to the influence of the yy components as well as due to certain nonuniformity of the static magnetization distribution, but the angle $\theta_M = 45^\circ$ remains a characteristic one for the formation of a well-defined field well. To sum up, if the theoretically calculated critical angle $\tilde{\theta}_M$ is smaller than 45° the presented theory can be applied; otherwise, the formation of edge modes should be accounted for (it may happen that in this case the mode merging phenomenon cannot be observed at all). In our case, $\tilde{\theta}_M < 45^\circ$ in a wide frequency range [see Fig. 6(c)]. In the general case, no restriction for $\tilde{\theta}_M$ to be smaller than 45° is found and such a case, maybe, could be realized for different relations between the dot thickness and the exchange length.

V. SUMMARY

In summary, we have studied the SWR spectra of obliquely magnetized thin circular magnetic nanodots and their evolution with the applied field angle θ_B variation. At certain critical angle $\tilde{\theta}_B$ of the bias magnetic field with respect to the dot normal, the SWR spectra become effectively single mode; instead of many SW modes visible in the spectra at other angles, only one prominent peak remains at $\tilde{\theta}_B$. Using micromagnetic simulations and an analytical theory, we have

found that the reason for this spectra transformation is the approximate degeneracy of many standing spin-wave modes at the transition of the spin-wave dispersion from the forward wave type to the backward one. Although such a transition is well known for continuous thin films, for nanodots it is found to be significantly affected by a nonzero quantized wave-number k_y in the direction perpendicular to the filed projection. Namely, nonzero k_y results in the observation of the mode merging at a significantly smaller tilt of static magnetization. The phenomenon of SW mode merging is observed for a wide range of nanodot diameters and could be useful for spectral narrowing of magnetic noise. For 40 nm-thick Permalloy dots this phenomenon disappears only for dots with diameters below 500 nm due to the too large intermode distance in k space, which makes impossible several modes to fall within a flat dispersion region at any field tilt.

ACKNOWLEDGMENTS

This work was supported by National Academy of Sciences of Ukraine, Grant No. 23-04/13-2021. The Portuguese team acknowledges the Network of Extreme Conditions Laboratories-NECL and Portuguese Foundation of Science and Technology (FCT) support through Projects No. NORTE-01-0145-FEDER-022096, No. POCI-0145-FEDER-030085 (NOVAMAG), and No. EXPL/IF/00541/2015. The support from the European Cooperation in Science and Technology via COST Action No. CA16218 (NANOCOHYBRI), from the Deutsche Forschungsgemeinschaft (DFG, German Research Foundation) via TRR 173/2 - 268565370 Spin + X: spin in its collective environment (Project B04), and from the Austrian Science Fund (FWF) through Grants No. I 4917-N (MagFunc) and No. I 4889 (CurviMag) is acknowledged. V.G. acknowledges support by National Research Foundation of Ukraine (Grant No. 2020.02/0261)

[1] *Spin Wave Confinement*, edited by S. O. Demokritov (Pan Stanford, Singapore, 2009).

[2] *Handbook of Surface Science*, edited by R. E. Camley, Z. Celinski, and R. L. Stamps (North-Holland, Amsterdam, 2016), Vol. 5.

[3] R. Verba, V. Tiberkevich, K. Guslienko, G. Melkov, and A. Slavin, Theory of ground-state switching in an array of magnetic nanodots by application of a short external magnetic field pulse, Phys. Rev. B. **87**, 134419 (2013).

[4] R. E. Camley, Three-magnon processes in magnetic nanoelements, Phys. Rev. B **89**, 214402 (2014).

[5] A. Etesamirad, R. Rodriguez, J. Bocanegra, R. Verba, J. Katine, I. N. Krivorotov, V. Tyberkevych, B. Ivanov, and I. Barsukov, Controlling magnon interaction by a nanoscale switch, ACS Appl. Mater. Interfaces **13**, 20288 (2021).

[6] R. Verba, L. Körber, K. Schultheiss, H. Schultheiss, V. Tiberkevich, and A. Slavin, Theory of three-magnon interaction in a vortex-state magnetic nanodots, Phys. Rev. B **103**, 014413 (2021).

[7] G. N. Kakazei, P. E. Wigen, K. Yu. Guslienko, V. Novosad, A. N. Slavin, V. O. Golub, N. A. Lesnik, and Y. Otani, Spin-wave spectra of perpendicularly magnetized circular submicron dot arrays, Appl. Phys. Lett. **85**, 443 (2004).

[8] I. Neudecker, K. Perzlmaier, F. Hoffmann, G. Woltersdorf, M. Buess, D. Weiss, and C. H. Back, Modal spectrum of permalloy disks excited by in-plane magnetic fields, Phys. Rev. B **73**, 134426 (2006).

[9] L. Giovannini, F. Montoncello, F. Nizzoli, G. Gubbiotti, G. Carlotti, T. Okuno, T. Shinjo, and M. Grimsditch, Spin excitations of nanometric cylindrical dots in vortex and saturated magnetic states, Phys. Rev. B **70**, 172404 (2004).

[10] G. Carlotti, Pushing down the lateral dimension of single and coupled magnetic dots to the nanometric scale: Characteristics and evolution of the spin-wave eigenmodes, Appl. Phys. Rev. **6**, 031304 (2019).

[11] K. Y. Guslienko, Magnetic vortex state stability, reversal and dynamics in restricted geometries, J. Nanosci. Nanotechnol. **8**, 2745 (2008).

[12] G. N. Kakazei, G. R. Aranda, S. A. Bunyaev, V. O. Golub, E. V. Tartakovskaya, A. V. Chumak, A. A. Serga, B. Hillebrands, and K. Y. Guslienko, Probing dynamical magnetization pinning in circular dots as a function of the external magnetic field orientation, Phys. Rev. B **86**, 054419 (2012).

[13] O. V. Dobrovolskiy, S. A. Bunyaev, N. R. Vovk, D. Navas, P. Gruszecki, M. Krawczyk, R. Sachser, M. Huth, A. V. Chumak, K. Y. Guslienko, and G. N. Kakazei, Spin-wave spectroscopy of individual ferromagnetic nanodisks, Nanoscale **12**, 21207 (2020).

[14] J. Jorzick, S. O. Demokritov, B. Hillebrands, M. Bailleul, C. Fermon, K. Y. Guslienko, A. N. Slavin, D. V. Berkov, and N. L. Gorn, spin Wave Wells in Nonellipsoidal Micrometer Size Magnetic Elements, Phys. Rev. Lett. **88**, 047204 (2002).

[15] K. Y. Guslienko, R. W. Chantrell, and A. N. Slavin, Dipolar localization of quantized spin-wave modes in thin rectangular magnetic elements, Phys. Rev. B **68**, 024422 (2003).

[16] C. Bayer, J. Jorzick, B. Hillebrands, S. O. Demokritov, R. Kouba, R. Bozinoski, A. N. Slavin, K. Y. Guslienko, D. V. Berkov, N. L. Gorn, and M. P. Kostylev, Spin-wave excitations in finite rectangular elements of $Ni_{80}Fe_{20}$, Phys. Rev. B **72**, 064427 (2005).

[17] G. Carlotti, G. Gubbiotti, M. Madami, S. Tacchi, and R. L. Stamps, Exchange-dominated eigenmodes in sub-100 nm permalloy dots: A micromagnetic study at finite temperature, J. Appl. Phys. **115**, 17D119 (2014).

[18] R. D. McMichael and M. D. Stiles, Magnetic normal modes of nanoelements, J. Appl. Phys. **97**, 10J901 (2005).

[19] J. Kharlan, P. Bondarenko, M. Krawczyk, O. Salyuk, E. Tartakovskaya, A. Trzaskowska, and V. Golub, Standing spin waves in perpendicularly magnetized triangular dots, Phys. Rev. B **100**, 184416 (2019).

[20] R. Arias, P. Chu, and D. L. Mills, Dipole exchange spin waves and microwave response of ferromagnetic spheres, Phys. Rev. B **71**, 224410 (2005).

[21] I. Neudecker, M. Kläui, K. Perzlmaier, D. Backes, L. J. Heyderman, C. A. F. Vaz, J. A. C. Bland, U. Rüdiger, and C. H. Back, Spatially Resolved Dynamic Eigenmode Spectrum of Co Rings, Phys. Rev. Lett. **96**, 057207 (2006).

[22] J. Podbielski, F. Giesen, and D. Grundler, Spin-Wave Interference in Microscopic Rings, Phys. Rev. Lett. **96**, 167207 (2006).

[23] F. Hoffmann, G. Woltersdorf, K. Perzlmaier, A. N. Slavin, V. S. Tiberkevich, A. Bischof, D. Weiss, and C. H. Back, Mode degeneracy due to vortex core removal in magnetic disks, Phys. Rev. B **76**, 014416 (2007).

[24] X. Zhou, E. V. Tartakovskaya, G. N. Kakazei, and A. O. Adeyeye, Spin wave modes in out-of-plane magnetized nanorings, Phys. Rev. B **96**, 024446 (2017).

[25] O. V. Dobrovolskiy, N. R. Vovk, A. V. Bondarenko, S. A. Bunyaev, S. Lamb-Camarena, N. Zenbaa, R. Sachser, S. Barth, K. Y. Guslienko, A. V. Chumak, M. Huth, and G. N. Kakazei, Spin-wave eigenmodes in direct-write 3D nanovolcanoes, Appl. Phys. Lett. **118**, 132405 (2021).

[26] M. Mruczkiewicz, M. Krawczyk, and K. Y. Guslienko, Spin excitation spectrum in a magnetic nanodot with continuous transitions between the vortex, Bloch-type skyrmion, and Néel-type skyrmion states, Phys. Rev. B **95**, 094414 (2017).

[27] V. P. Kravchuk, D. D. Sheka, U. K. Rößler, J. van den Brink, and Y. Gaididei, Spin eigenmodes of magnetic skyrmions and the problem of the effective skyrmion mass, Phys. Rev. B **97**, 064403 (2018).

[28] S. A. Bunyaev, V. O. Golub, O. Yu. Salyuk, E. V. Tartakovskaya, N. M. Santos, A. A. Timopheev, N. A. Sobolev, A. A. Serga, A. V. Chumak, B. Hillebrands, and G. N. Kakazei, Splitting of standing spin-wave modes in circular submicron ferromagnetic dot under axial symmetry violation, Sci. Rep. **5**, 18480 (2015).

[29] F. G. Aliev, J. F. Sierra, A. A. Awad, G. N. Kakazei, D.-S. Han, S.-K. Kim, V. Metlushko, B. Ilic, and K. Y. Guslienko, Spin waves in circular soft magnetic dots at the crossover between vortex and single domain state, Phys. Rev. B **79**, 174433 (2009).

[30] D. A. Bozhko, H. Yu. Musiienko-Shmarova, V. S. Tiberkevich, A. N. Slavin, I. I. Syvorotka, B. Hillebrands, and A. A. Serga, Unconventional spin currents in magnetic films, Phys. Rev. Res. **2**, 023324 (2020).

[31] R. V. Verba, A. Hierro-Rodriguez, D. Navas, J. Ding, X. M. Liu, A. O. Adeyeye, K. Y. Guslienko, and G. N. Kakazei, Spin-wave excitation modes in thick vortex-state circular ferromagnetic nanodots, Phys. Rev. B **93**, 214437 (2016).

[32] A. Helmer, S. Cornelissen, T. Devolder, J.-V. Kim, W. van Roy, L. Lagae, and C. Chappert, Quantized spin-wave modes in magnetic tunnel junction nanopillars, Phys. Rev. B **81**, 094416 (2010).

[33] O. Klein, G. de Loubens, V. V. Naletov, F. Boust, T. Guillet, H. Hurdequint, A. Leksikov, A. N. Slavin, V. S. Tiberkevich, and N. Vukadinovic, Ferromagnetic resonance force spectroscopy of individual submicron-size samples, Phys. Rev. B **78**, 144410 (2008).

[34] K. Yu. Guslienko, S. O. Demokritov, B. Hillebrands, and A. N. Slavin, Effective dipolar boundary conditions for dynamic magnetization in thin magnetic stripes, Phys. Rev. B **66**, 132402 (2002).

[35] K. Yu. Guslienko and A. N. Slavin, Boundary conditions for magnetization in magnetic nanoelements, Phys. Rev. B **72**, 014463 (2005).

[36] Q. Wang, B. Heinz, R. Verba, M. Kewenig, P. Pirro, M. Schneider, T. Meyer, B. Lägel, C. Dubs, T. Brächer, and A. V. Chumak, Spin Pinning and Spin-Wave Dispersion in Nanoscopic Ferromagnetic Waveguides, Phys. Rev. Lett. **122**, 247202 (2019).

[37] In this ideal case SW profiles are of the form $\cos[2n\pi x/L]$ and $\sin[(2n+1)\pi x/L]$, $n = 0, 1, 2, \ldots$ for symmetric and antisymmetric modes, respectively; $x \in [-L/2, L/2]$. Net dynamic magnetic moment is present only for the lowest symmetric mode (with $n = 0$).

[38] A. Vansteenkiste, J. Leliaert, M. Dvornik, M. Helsen, F. Garcia-Sanchez, and B. Van Waeyenberge, The design and verification of MuMax3, AIP Adv. **4**, 107133 (2014).

[39] K. Yu. Guslienko and A. N. Slavin, Spin-waves in cylindrical magnetic dot arrays with in-plane magnetization, J. Appl. Phys. **87**, 6337 (2000).

[40] R. Zivieri and R. L. Stamps, Theory of spin wave modes in tangentially magnetized thin cylindrical dots: A variational approach, Phys. Rev. B **73**, 144422 (2006).

[41] B. A. Kalinikos and A. N. Slavin, Theory of dipole-exchange spin wave spectrum for ferromagnetic films with mixed exchange boundary conditions, J. Phys. C **19**, 7013 (1986).

[42] K. Y. Guslienko and A. N. Slavin, Magnetostatic Green's functions for the description of spin waves in finite rectangular magnetic dots and stripes, J. Magn. Magn. Mater. **323**, 2418 (2011).

[43] S. Tandon, M. Beleggia, Y. Zhu, and M. De Graef, On the magnetostatic interactions between nanoparticles of arbitrary shape, J. Magn. Magn. Mater. **271**, 9 (2004).

[44] R. I. Joseph, Ballistic demagnetizing factor in uniformly magnetized cylinders, J. Appl. Phys. **37**, 4639 (1966).